JOURNAL OF GEOPHYSICAL RESEARCH, VOL. 86, NO. A7, PAGES 5715-5725, JULY 1, 1981

Composition and Thermal Profiles of the Jovian Upper Atmosphere Determined by the Voyager Ultraviolet Stellar Occultation Experiment

M. C. FESTOU, S. K. ATREYA,[1] AND T. M. DONAHUE

Space Physics Research Laboratory, Department of Atmospheric and Oceanic Science, The University of Michigan Ann Arbor, Michigan 48109

B. R. SANDEL, D. E. SHEMANSKY, AND A. L. BROADFOOT

Earth and Space Sciences Institute, Tucson, Arizona 85713

Occultation of the star Regulus—α Leo—by the Jovian atmosphere was monitored by the Voyager 2 spacecraft on July 9, 1979. The absorption recorded in the 910–1200 Å range was caused primarily by the H_2-Lyman and Werner bands. These data provide the first complete measurements of atmospheric density and temperature profiles between 330 and 830 km above the ammonia cloud tops. The molecular hydrogen density at 380 km is found to be $3^{+4}_{-1} \times 10^{13}$ cm^{-3}, where the atmospheric temperature is 200 ± 50 K. The thermal gradient above 830 km altitude is found to be approximately 1 K km^{-1} to reconcile the stellar occultation data with the Voyager 1 solar occultation data for the exosphere. Both experiments were performed in the equatorial region. The observed temperature gradient in the upper atmosphere rules out inertia gravity wave propagation as the primary heating mechanism; the heating must be caused by one or many of a host of other potential sources such as magnetospheric electrons (soft or hard), Joule heating and even solar extreme ultraviolet radiation. The data do not present a strong argument in favor of an earthlike mesopause on Jupiter. The absorption in the 1250–1600 Å range yields volume mixing ratios of methane and ethane of $2.5^{+3}_{-2} \times 10^{-5}$ and $2.5^{+2.0}_{-1.5} \times 10^{-6}$, respectively, at a height of 325 km above the ammonia cloud tops. An upper limit of 2.5×10^{-6} for the mixing ratio of acetylene has been found at the altitude of 300 km. The Voyager infrared data yield mixing ratios of these hydrocarbons deeper in the stratosphere. A study of the density profiles of the hydrocarbons deduced from the stellar occultation data yields a value of the eddy diffusion coefficient at the homopause to be $1.4^{+0.8}_{-0.7} \times 10^6$ cm^2 s^{-1} in the equatorial region which is consistent with the value deduced from the hydrogen Lyman alpha and helium 584 Å emission data. Detailed aeronomical implications of the results are discussed elsewhere (Atreya et al., 1981).

A. INTRODUCTION

The ultraviolet spectrometer (UVS) of the Voyager spacecraft was designed to determine the composition and structure of the atmospheres of Jupiter, Saturn, and their satellites. Two operational modes are available: the airglow mode, which provides measurements of the emissions from the atmospheres, and the occultation mode, which measures atmospheric extinction of stellar or solar radiation. The extinction is characteristic of the atmospheric composition and thus allows us to trace those species which absorb within the observing wavelength range. The density of H_2 at the deepest level probed in this experiment is 3×10^{14} cm^{-3}, and the line of sight column density is 1.2×10^{23} cm^{-2} at that altitude. Refraction and Rayleigh scattering effects are therefore unimportant and not included in this analysis. The advantage of the occultation technique lies in the fact that the results are dependent only on the ratio of the unattenuated signal (measured prior to the atmospheric absorption) to the signal attenuated on absorption by the atmospheric gases. Knowledge of the absolute flux or instrument calibration are not required.

The UVS instrument (section B) is an objective grating spectrometer covering the wavelength range 510–1690 Å in contiguous 10 Å channels. In this wavelength interval, most atmospheric species have very strong absorption features (H, H_2, He, CH_4, C_2H_2, C_2H_6). Because of large angular diameter of the Sun (0.1° at 5.2 AU) and the relatively large range of the Voyager spacecraft from Jupiter, the solar occultation experiment provided only limited information (such as temperature) in the exosphere. On the other hand, an occultation of a star—which is a discrete point source—permits a measurement of molecular hydrogen and most hydrocarbons deep in the atmosphere. During the occultation of the star Regulus (B7 type) by Jupiter as seen from the Voyager 2 spacecraft on July 9, 1979, two absorbing regions were clearly detected (section C). Between 911 and 1200 Å, H_2 was absorbing over a 600 km altitude range (section D). Above 1300 Å, the rapid increase of the absorption by the hydrocarbons was observed over an altitude interval of ~100 km with a height resolution of 3 km (section D). The analysis of these absorption features has provided the height profiles of molecular hydrogen, methane, ethane and acetylene, as well as the thermal profile in the upper atmosphere of Jupiter (sections D and E).

Combining the Voyager UVS results with other data, such as those obtained by the Voyager infrared and radioscience instruments, has yielded a comprehensive model of the composition and structure of the atmosphere of Jupiter.

B. OBSERVATIONS

1. *Instrument Capabilities*

A detailed description of the Voyager ultraviolet spectrometer (UVS) is given elsewhere [*Broadfoot et al.*, 1977]. Only those details of the instrument which are relevant to this paper are presented here. The instrument is an objective grating

[1] Send reprint requests to S. K. Atreya.

Paper number 1A0339.
0148-0227/81/001A-0339$01.00

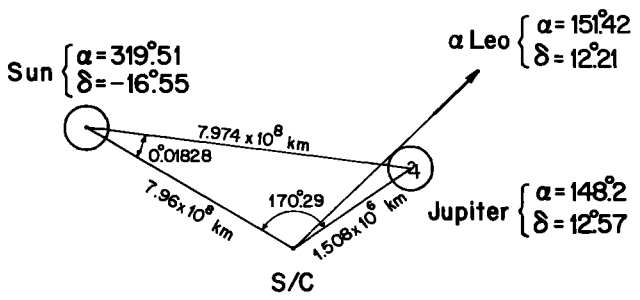

Fig. 1*a*. Geometrical parameters at occultation time t_o = July 9, 1979, 0246:24. All coordinates refer to 1950.0.

spectrometer covering the range 510–1690 Å. A mechanical collimator restricts the field of view (FOV) in the dispersion direction of the grating to 0.1° (full width at half maximum (FWHM)) while it is limited in the perpendicular direction by the width of the detector in the image plane (0.87°). Spectral and spatial resolutions are not independent. A spatially extended emission line which fills the FOV produces a triangular intensity distribution with a FWHM of 0.1°, which corresponds to a 33.1 Å spectral width. On the other hand, a monochromatic point source produces a linewidth of 25 Å. The detector channels have a width of 0.028° or 9.26 Å.

The photon counting detector is composed of a 128 element array which collects the output of a dual microchannel plate electron multiplier [*Broadfoot and Sandel*, 1977]. The array detector, when illuminated by a uniform field of electrons, produces a signal which varies from anode to anode; this 'fixed pattern noise' has been measured with an accuracy of 1% and all our data have been corrected for this effect.

Since in these observations we are dealing with relative measurements, we shall not examine the question of the absolute instrumental sensitivity (which can be found in the work of *Shemansky et al.* [1979]). However, it should be noted that the peak sensitivity of the UVS is around 600 Å in order to favor the short wavelengths; this sensitivity curve is shown in the work of *Broadfoot et al.* [1981]. Both grating efficiency and channel plate efficiency drop toward longer wavelengths and the instrumental sensitivity decreases by about a factor of 10 at 1100 Å and by about a factor of 50 above 1400 Å. As a consequence, statistical uncertainties in the data increase at longer wavelengths.

The instrumental scattering matrix (or instrumental response to a monochromatic source at any wavelength) has been determined for 50 wavelengths throughout the total spectral range. The scattering spectrum of a monochromatic spatially extended emission line centered at 1216 Å is shown by *Broadfoot et al.* [1981], and its FWHM is 33 Å. We have checked at several wavelengths and found that the effects of instrument internal scattering have practically no influence on our experimental results. Consequently, the data used in the present analysis have not been corrected for this effect. In the pressure regime of the present observations ($P \lesssim 10$ μbar), the effect of haze—such as seen at the millibar or higher pressures [*Cook et al.*, 1979; *Smith et al.*, 1977]—is unimportant.

2. *Data Collection*

During the ultraviolet stellar occultation experiment, the scan platform of the spacecraft was directed toward the star Regulus (α Leonis, HD 87901. B7V, $V = +1.35$) and then fixed in position with respect to the spacecraft. Two motions of the spacecraft result in a change of the position of the star in the FOV. First, the three axis pointing system of the spacecraft scan platform has a limit cycle of ±0.05° in occultation mode. Second, a slow drift results from the motion of the spacecraft on its trajectory.

The occultation of α Leo by Jupiter occurred when the Voyager 2 (V2) spacecraft was 1.5×10^6 km from the planet (Figure 1*a*). During the first phase of observations, 3000 spectra (integration time of 0.32 s per spectrum) were taken before the line of sight joining the star to the spacecraft reached the Jovian limb. The first 2700 spectra were unattenuated spectra of α Leo as recorded by V2-UVS. In a second phase, the spacecraft swung behind the planet while the spectrometer was continuously directed toward the star. The stellar light was then progressively absorbed as the tangent ray to the star descended at ~10 km s^{-1} to deeper layers in the atmosphere. Four hours after this 'ingress,' the star appeared again in the instrumental slit ('egress').

The ingress phase lasted approximately one minute, which corresponds to a vertical path of the line of sight through the Jovian atmosphere of ~600 km (Figure 1*b*). The limit cycle motion was well controlled and the star remained within 0.05° of the center of the slit. On the other hand, during egress, the amplitude of the limit cycle had increased and the star was on the edge of the FOV causing a significant reduction of the recorded signal. In addition, the noise induced by the Jovian electrons had increased by a factor of two, both effects led to a poor signal to noise ratio. Because of extremely poor statistics the egress data have not been analyzed.

The positions and dimensions of the projection of the slit at the distance of Jupiter are shown in Figure 1*b*: the slit half width corresponds to 2620 km while its length is 22,800 km. The spatial resolution is determined by the integration time of 0.32 s which corresponds to a change in the position of the line of sight of 3.2 km. The first contact of the slit with the Jovian disc occurred 810 s before occultation time 't_o' which we define as the time when the stellar signal drops to the background noise level in the 1281–1393 Å wavelength interval (see Figure 3*a*, below). The slit was completely on the disc 950 s after t_o. These numbers are 13.5 and 16 times larger than the occultation duration of one minute. During the occultation

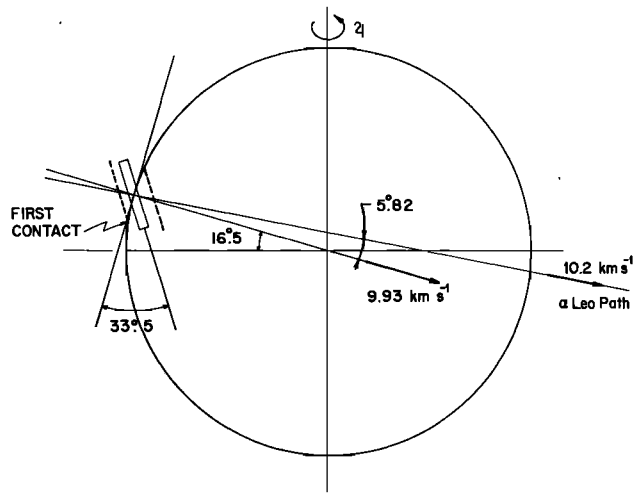

Fig. 1*b*. Position and dimension of the instrument slit at occultation time.

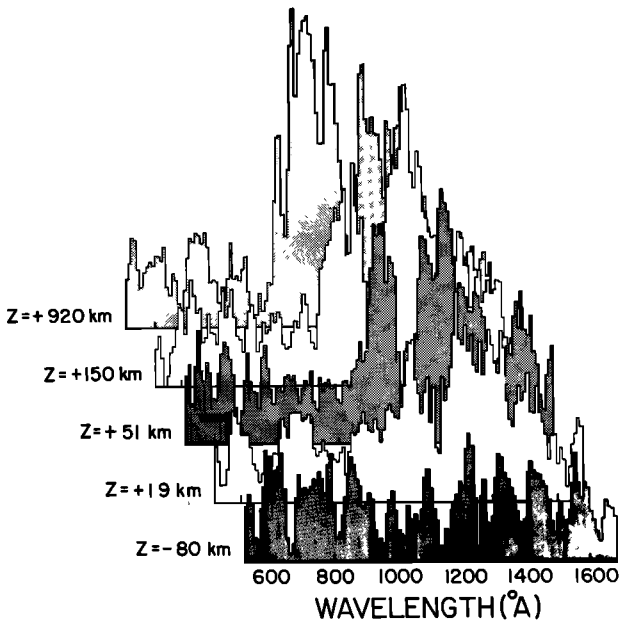

Fig. 2. Spectra taken at various altitudes in the Jovian atmosphere. Each spectrum is the average of ten individual spectra so that the actual range of altitudes covered shows a dispersion of ±16 km around the indicated values. The altitudes refer to z_{t_0} which is approximately 330 km above the ammonia cloud tops which are located at ~600 mbar, T = 150 K.

period, the portion of the slit covering the Jovian disc remained constant within ±3%.

C. Data Analysis

1. *Data Content*

The basic data are composed of spectra of the star seen through the Jovian atmosphere with an altitude resolution of 3.2 km. For illustration, we show in Figure 2 spectra averaged over 3.2 s or 32 km and at various altitudes which refer to the total exinction level at time t_o. The average spectrum marked by z = 920 km is an unattenuated stellar spectrum. The decrease of the signal above 1200 Å is the result of the low response of the instrument at these wavelengths.

A second way to present the data consists of following the evolution of the attenuated stellar signal with a spectral resolution of 10 Å. In that way we obtain a 'light curve.' If the signal is normalized with respect to the unattenuated stellar signal, we obtain an 'absorption curve' measured from the total extinction level z_{t_0} = 0 km at time t_o. Once the H_2 density at z_{t_0} has been determined from the data analysis, we can relate the altitude z_{t_0} to a more convenient reference, the ammonia cloud tops—as has been done in section D1*b*. All data reduction figures (Figures 1–5) are referenced to the height z_{t_0}. Figures 7, 8 and 9 show altitudes above the ammonia cloud tops. Figures 3*a* and 3*b* show two very different light curves corresponding to the addition of the signal over 12 and 11 consecutive channels, respectively. As we shall show below, the shape of these two light curves is determined by the absorption by hydrocarbons and by molecular hydrogen. For illustration, we show in Figure 3*c* a breakdown of the signal of Figure 3*b* (Figure 3*a* could be decomposed in the same way). The signal is characterized by four components: (1) component 1—stellar signal only seen before t_o; (2) component 2—the interplanetary background whose contribution can be recorded until time t_o + 950 s, as long as a part of the slit is outside the planetary disc; (3) component 3—the eventual emission from the Jovian disc which may contribute after time t_o − 810 s, when a part of the slit is on the planetary disc; (4) component 4—the noise induced by energetic Jovian electrons. The diffuse EUV emission from the interstellar medium as well as the Io torus emission can be neglected [*Sandel et al.*, 1979]. The four components of the signal are highly variable. The stellar contribution depends on the position of the line of sight in the Jovian atmosphere. The interplanetary emission is dominated by the He 584 Å, H Ly β (1025 Å) and H Ly α (1216 Å) lines [*Shemansky et al.*, 1979]. Owing to the small angular variation of the position of the line of sight around t_o (less than ±10 arc minutes), these emissions can be considered as constant. As can be seen in Figure 1*a*, the phase angle of Jupiter at occultation time is ~9°. Then, one can expect to record, together with the stellar and interplanetary spectra, the dayside emissions of the Jovian disc [*Sandel et al.*, 1980] which are dominated by a strong H Ly α line. The other important emissions are the Lyman and Werner bands of H_2, the H Ly β line and a rather weak feature around 1570 Å. With the exception of the H Ly α line at 1216 Å, none of these emissions produces more than 0.3 count per 0.32 s per channel in the equatorial region where the stellar occultation took place. The actual counting rate, however, is only 1/2 of 0.3 count per 0.32 s, since only half the slit was on the disc. The unattenuated counting rate from the star is, on the other hand, about 2 counts per 0.32 s per channel. The noise induced by energetic electrons depends strongly on the position of the spacecraft with respect to the Jovian magnetic equator. This effect has been investigated on a long-term basis [*Broadfoot et al.*, 1981] as well as from the direct study of the occultation data. It has, therefore, been possible to remove this important component from the signal but short time scale variations may still remain. One of those unfortunate variations occurred almost exactly during the egress and resulted in the loss of all egress data for $\lambda > 1100$ Å.

2. *Correction of the Raw Spectra*

All experimental spectra are first corrected for the fixed pattern noise defined in section B1. The rate of increase of background around time t_o was determined from a study of the first 5000 spectra taken after the stellar signal was absorbed ($t > t_o$). The long-term study showed that a linear increase was a good approximation. A background spectrum has been obtained by averaging 350 spectra taken 900 s after t_o, when the slit was entirely on the disc, so that the signal was only composed of two components, the electron induced noise and the Jovian airglow. An examination of all corrected spectra for $t > t_o$ showed that no significant emission other than the Ly α line was present in our background spectrum since no correlation appeared between the fraction of the slit which was on the disc (from 50% to 100%) and the measured count rate: all variations around the zero level are random.

We were then able to correct the spectra obtained before t_o. The signal has two components, the stellar light which is more or less absorbed and the interplanetary emission. In the following we shall analyze the spectral region λ912–1615 Å; spectral regions around the Ly β (1004–1041 Å) and Ly α (1189–1245 Å) lines have not been considered since the signal at these wavelengths comprises of the Jovian and the interplanetary emissions. Consequently, we are left with a theoreti-

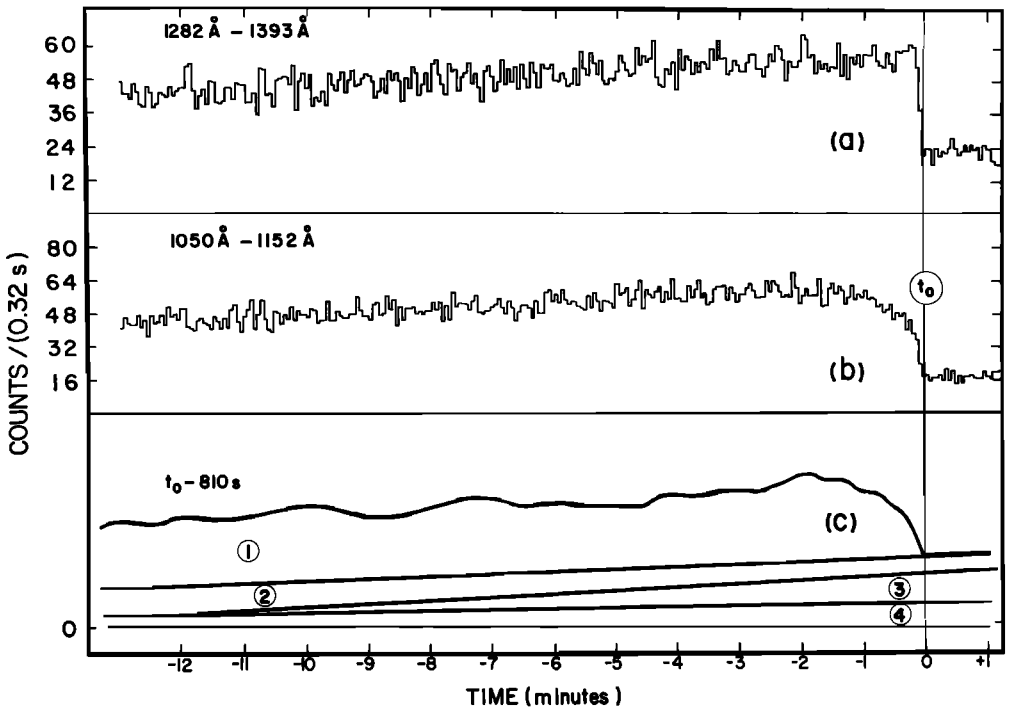

Fig. 3. Light curves obtained by a double compression of the data. Each point represents the average number of counts in the indicated wavelength interval computed from ten individual spectra. (*a*) Absorption by the hydrocarbons, the time t_0 corresponds to a total extinction in this wavelength interval, (*b*) Absorption by H_2. (*c*) Different possible components of the recorded signal—see the text for the explanation of the nature of these components.

cally pure stellar signal. Two effects expected as a consequence of the instrumental characteristics described above are easily observed in the data:

1. When the position of α Leo in the slit changes, the total signal recorded varies. Approximately 2000 unattenuated stellar spectra (0.32 s integration times) were available to investigate this effect and correct the data.

2. When a typical feature (the side of the Ly β line, for example) is followed, the spectral location changes with the position of the star. A displacement of 3.3 ± 0.3 diodes per 0.1° in the direction perpendicular to the slit (elevation) was determined. No change in the direction parallel to the slit (azimuth) was observed. The elevation displacement value is in very good agreement with the expected value of 0.028°/element. This effect will be negligible if the elevation does not change by more than ±0.005°, a condition which has been fulfilled during the entire occultation period.

We have obtained a 'stellar reference' spectrum from 200 individual spectra taken when the line of sight was 7×10^3 km above the planet limb. It is very similar to the spectrum shown at the top of Figure 2. All spectra have been corrected by a factor depending on the position of the star in the slit. Then, we have divided them by the reference spectrum in order to obtain the absorption spectra.

3. *Experimental Results*

In all, seventy three absorption curves are available with an altitude resolution of 3.2 km. The average count rate is 1 to 3 counts per 0.32 s and per channel. The resulting statistics are relatively poor and, depending on the goal which is to be reached, one is obliged to sacrifice either the altitude resolution by adding consecutive spectra together, or the spectral resolution by adding contiguous channels together. The spectra displayed in Figure 2 are an illustration of the integration in time: the short wavelength portion of the stellar spectrum ($\lambda <$ 1150 Å) is slowly absorbed while the long wavelength portion ($\lambda >$ 1300 Å) is absorbed only within the last few seconds. These characteristics are associated with the absorption by molecular hydrogen and hydrocarbons respectively.

A close examination of all individual spectra reveals the following physical characteristics in the data:

1. Below 1200 Å and at an altitude larger than 30 km, the detected absorption is due to molecular hydrogen, H_2. We have added together all contiguous absorption curves showing the same time dependence within the statistical uncertainties. Three wavelength intervals were necessary to cover the 912–1189 Å region—the results are shown in Figure 4. The 912–1004 Å region provides an absorption curve very similar to the one resulting from the integration over the 1041–1106 Å interval. However, the latter curve is much better defined from the statistical point of view. The curve for the 1106–1189 Å region indicates that the absorption takes place between approximately 0 and 70 km.

However, the examination of the individual light curves show that, within the experimental uncertainties, the transmission goes from 40% to 0% over a 10 km altitude range centered at 8 ± 6 km. This sudden increase in the absorption can be explained by examining the following approximation for the transmitted intensity at a given wavelength:

$$I = I_0 \exp\left\{-\tau_0 \exp\left[-\frac{z - z_0}{H}\right]\right\} \quad (1)$$

where τ_0 is the optical depth at level z_0, H is the scale height of the atmosphere (assumed to be constant for the sake of simplicity). Therefore, a sudden increase of the I/I_0 ratio can

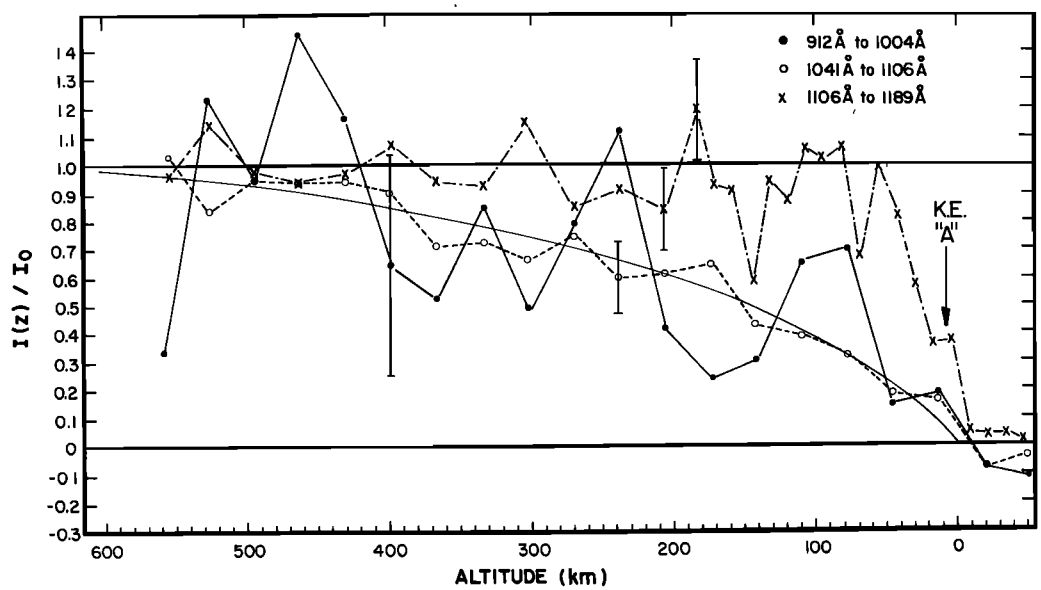

Fig. 4. Absorption by molecular hydrogen (above z_{t_0} + 30 km when $\lambda \gtrsim 1100$ Å). The origin of the altitude scale corresponds to the time t_0 shown in Figure 3. The absorption is nearly independent of the wavelength below 1106 Å but it behaves differently above this limit which is defined to within ±20 Å. The altitude resolution is 32 km, except in the 0–200 km region for the 1106–1189 Å wavelength interval where it is 12 km. However, the knife edge '*A*' mentioned in the text is not apparent here because of the height resolution.

only be explained by a corresponding fast increase of the scale height *H*. This is called a 'knife edge effect' (K.E.).

It will be shown in section D that this knife edge at 8 ± 6 km cannot be produced by H_2. The knife edge is referenced 'A' in Figure 5.

2. Above 1250 Å, the absorption takes place over 120 km, at most. The absorption can be either 'smooth,' i.e., no sudden decrease of the transmitted signal, or have a knife edge appearance. Very few consecutive channels behave in the same manner so that any integration over large wavelength intervals would result in a loss of information.

Figure 5 exhibits for each channel above 1254 Å the level at

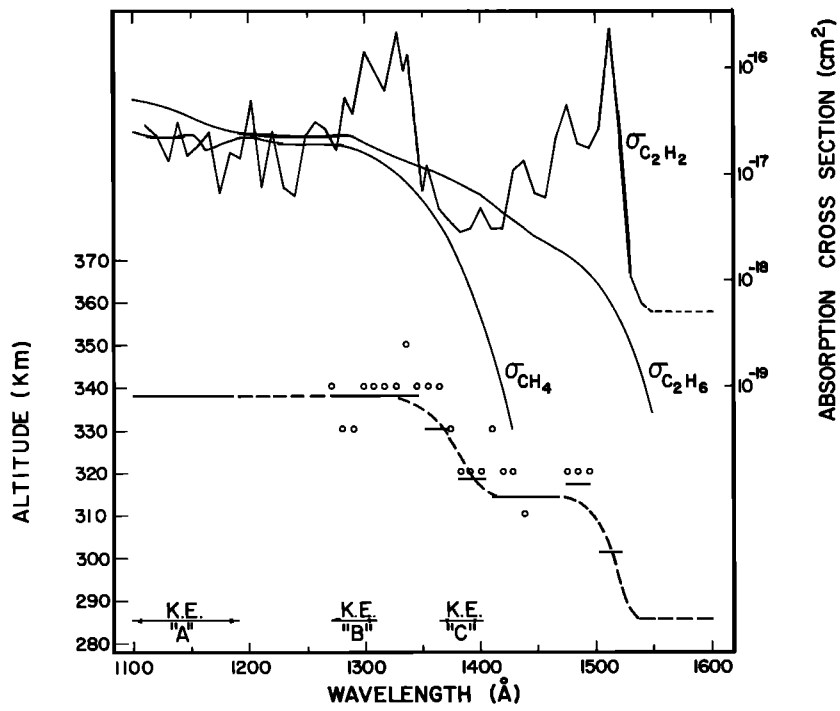

Fig. 5. Fifty percent absorption levels for individual channels (dots) and a few sets of channels (straight lines). The broken line represents the general trend. The wavelength range of the three knife edges (see text) is shown by the arrows; their corresponding locations can be read off the curve (see also Figure 8). The absorption cross sections of methane, ethane, and acetylene (averaged over 9.26 Å wavelength intervals) are indicated in the upper part of this figure.

TABLE 1. Relationships Between Rotational and Vibrational Transition Probabilities

Branch	$A_{J'J''}/A_{v'v''}$
H_2 Werner Bands	
$P(J+1)$	$J/(2J+1)$
$Q(J)$	1
$R(J-1)$	$(J+1)/(2J+1)$
H_2 Lyman Bands	
$P(J+1)$	$(J+1)/(2J+1)$
$R(J-1)$	$J/(2J+1)$

which 50% absorption of the signal takes place. The horizontal bars represent this level for a few sets of consecutive channels, which help to understand the general trend shown by the broken line curve. The average altitude resolution for the sets is ±9 km and for individual channels the experimental uncertainty may be as high as ±18 km. Above 1530 Å, we were even obliged to sum all channels together because of the very low level of the recorded stellar signal (see, e.g., Figure 2). Whenever a knife edge is identified by examining the individual light curves, it has been indicated by 'K.E.,' while in all other cases the absorption is smooth. It should be emphasized that a knife edge effect can be considered as real only if it occurs in three or more consecutive channels since a single photon event is detected by the three adjacent diodes. Therefore, the demonstration of the existence of the three knife edges mentioned in Figure 5 would require displaying at least thirty individual light curves—which is not practical. The reader can get an idea of the appearance of a knife edge by examining the data in Figures 3*a* and 3*b* in which the quickness of the decrease in the signal around time t_0 is due to the fact that some individual light curves showing a knife edge effect are included in the summations. Strong departures from the broken line of Figure 5 around $\lambda = 1340$ Å or 1410 Å are probably caused by the statistical noise.

D. Data Interpretation

We have seen in the preceeding section that the absorption by molecular hydrogen could be separated from the absorption by any other species provided that we restrict ourselves to altitudes above 30 km and wavelengths below 1200 Å. In the following section, we shall analyze our experimental data relating to H_2 (Figure 4) separately from that relating to the hydrocarbons (Figure 5) and we shall determine a posteriori that this separation is a reasonable working assumption.

1. *Molecular Hydrogen*

a. Absorption by H_2. The only significant absorption by H_2 in the 912–1200 Å region is due to the Lyman and Werner bands which connect the ground state $X\,{}^1\Sigma_g^+$ with the excited states $B^1\Sigma_g^+$ and $C^1\Pi_u$. We have computed the atmospheric transmission at frequency ν through an atmosphere of thickness l assuming that each individual vibration-rotation line could be considered as having a Voigt profile (natural and Doppler broadenings only). First order scattering equations (optically thin atmosphere) have been applied to the calculations, and the transmitted intensity $I(\nu)$ is described in the equation

$$I(\nu) = I_0(\nu) \exp\left[-\sum_{J'J''v'v''} k(\nu)\, l\right] \tag{2}$$

where l is the depth of the gas in cm and $k(\nu)$ is the absorption coefficient in cm^{-1}. The function $k(\nu)$ in this case is defined by the well-known Voigt function, $K(x, y)$:

$$k(\nu) = k_0 K(x, y) \tag{3}$$

where

$$x = \frac{\nu - \nu_0}{\alpha_D} (\ln 2)^{1/2} \tag{4}$$

$$y = \frac{\alpha_L}{\alpha_D} (\ln 2)^{1/2} \tag{5}$$

ν_0 is the line center wavenumber for a given fine structure transition and α_L and α_D are the Lorentz and Doppler line widths. The summation in (2) is made over all bands of the two systems for which calculated molecular data are available, constituting essentially all of the measurable absorption. The quantity k_0 for a given line is directly related to the integrated line strength $S^{J''J'}$ by the equation

$$S^{J''J'} = \alpha_D \left(\frac{\pi}{\ln 2}\right)^{1/2} k_0 = h\nu_0 B_{J''J'} N_{J''} \tag{6}$$

where $B_{J''J'}$ is the Einstein absorption probability for a given $J''J'$ transition of a particular band and $N_{J''}$ is the lower level rotational population density. The lower state population is assumed to be in a Maxwell-Boltzmann distribution, taking into account ortho-para partitioning. The relationship between fine structure transitions, $A_{J'J''}$, and band transition probabilities, $A_{v'v''}$, is a simple one since both electronic systems are spin allowed transitions. All rotational levels of a given upper state vibrational level, therefore, have the same lifetime, although lifetimes vary as a function of upper vibrational quantum numbers. The relationship between $A_{J'J''}$ and $A_{v'v''}$ for the two band systems is shown in Table 1. Note that the quantities refer to the fine structure transitions and, therefore, the Q branch transitions in the case of the Werner system do not arise from the same rotational levels as the P and R branch lines (Λ-splitting). The relationship between the known $A_{v'v''}$ values and the fine structure absorption probabilities, $B_{J''J'}$, are then directly determined through Table 1 by the usual equations [*Herzberg*, 1959] which relate absorption and transition probabilities, but including only the degeneracy due to rotation [*Shemansky*, 1969].

Band transition probabilities and upper state lifetimes as a function of vibrational level were obtained from *Allison and Dalgarno* [1970] and *Dalgarno and Stephens* [1970]. The usual equations for vibrational energy were not adequate for the required accuracy, and tabulated values were used from the data reductions of *Dabrowski and Herzberg* [1974], *Wilkinson* [1968], *Namioka* [1964] and *Herzberg and Howe* [1959]. Rotational and electronic constants were obtained from the same sources.

The transmitted signal was computed by adding extinction coefficients given by (2) over wavelength intervals in which the incoming stellar spectrum can be assumed constant. Then, this signal was convolved with the instrument function, multiplied by the unattenuated stellar spectrum and compared with the data after averaging over the appropriate wavelength interval.

Figure 6 illustrates the most important characteristics of the Lyman and Werner band absorptions:

1. The measured absorption coefficient in the 150–2000 K

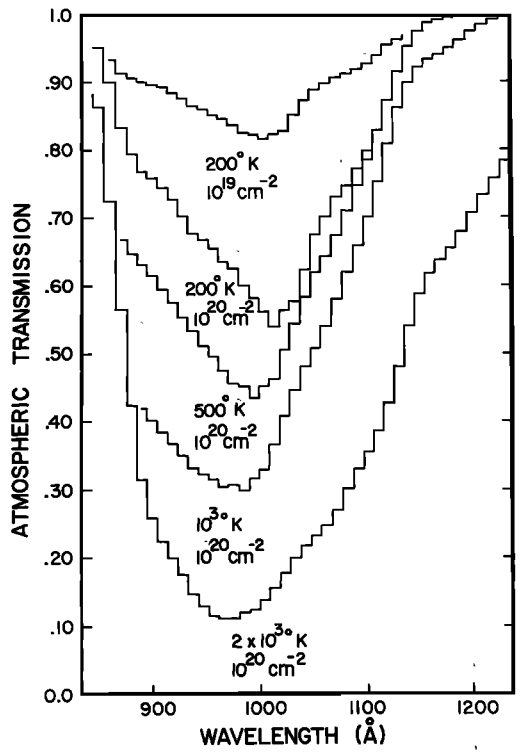

Fig. 6. Atmospheric transmission (as the Voyager 2 UVS would measure it) for isothermal lines of sight characterized by the indicated temperature and column densities.

range has a maximum around $\lambda = 960$ Å. The higher the column density, the higher is the peak of the absorption coefficient.

2. Relative to the short wavelength side, the long wavelength side of the absorption coefficient function is more affected by a change in the column density than by a change in the temperature.

b. Thermal and density distributions. In order to perform the calculations presented in section D1*a* we assume models of both the thermal and density distributions in the Jovian atmosphere. In calculating the absorption coefficients, $k(\nu)$, we take into consideration temperature variation along the line of sight. Comparing the absorption as a function of altitude and wavelength computed from the models with the data provides a unique set of both temperature and density distributions. Since the lines of sight were almost perpendicular to the rotation axis of the planet and since they were passing close to the equatorial plane, we have assumed spherical symmetry.

The wavelength interval λ912–1004 Å has the highest absorption for a given column density and therefore appears to be the most appropriate to study the upper atmosphere. Unfortunately, the data are very noisy. Thus, we were forced to use the wavelength interval λ1041–1106 Å which is sensitive to both column density and temperature. We fix the temperature profile and then determine the range of column densities at 50 km which fit the data. In the wavelength interval 1106–1189 Å, the range of altitudes over which the absorption takes place (less than 100 km) is too small to be sensitive to the actual shape of the temperature distribution (but it is sensitive to the average temperature), so we use those data to reduce the uncertainty of the value of the column density previously determined.

The lack of absorption above 100 km in this last curve (1106–1189 Å) can be interpreted to give an upper limit for the column density as a function of the temperature which we assume for this test to be constant. The upper limits corresponding to 200 K, 500 K, 1000 K, and 2000 K are 10^{21} cm^{-2}, 1.8×10^{19} cm^{-2}, 5×10^{17} cm^{-2}, and 7×10^{16} cm^{-2}, respectively—all these combinations produce a 5% absorption. On the other hand, these isothermal profiles would produce at the same level, in the 1041–1106 Å region, absorptions of 42%, 80%, 91%, and 95%, respectively. The actual observed value is 40%, so that one can expect a cold and dense atmosphere around the 100 km level: the weak absorption above 100 km means that no atmospheric layer above this level contributes significantly to the total absorption. Thus, the above combinations of parameters relate necessarily to the 0–100 km region for which an isothermal atmosphere in the 150–250 K range is a good assumption.

We have used the 1106–1189 Å light curve to determine the column density at 50 km. The absorption at this level depends strongly on the column density, as seen in section D1*a*, and very little on the temperature which has been taken equal to 200 ± 50 K, as it results from the above study. The column density at 50 km is found to be $1.4^{+1.4}_{-0.7} \times 10^{22}$ cm^{-2}.

Next, we consider the 1041–1106 Å light curve (full line in Figure 4) in order to determine the temperature and density profiles in the 50–500 km range. We have first tested isothermal profiles: a reasonably good agreement with the observations, but not a fit, could be obtained as long as the temperature did not exceed 250 K. From the departure between the models and the data, we conclude that the simplest temperature profile likely to represent the observations would consist of a constant temperature in the lower part of the atmosphere and a linearly increasing temperature in the upper part up to the exosphere. Provided that the highest temperature is reached at an altitude at least as high as 800 km, a value which will be determined below by an independent analysis, the value of the maximum does not play any role in the absorption below 500 km. We are, therefore, left with the following variable parameters for the above mentioned profile: (1) the number density at 50 km, (2) the temperature of the lower atmosphere, and (3) the altitude of the turn around point above which the temperature increases with a gradient which is to be determined. Numerous profiles have been tested, keeping in mind that the column density at 50 km is known. The following results were obtained: (1) the altitude of the turn around point is 100 ± 50 km; (2) the corresponding extremum temperatures below this point are 210 ± 30 K and 190^{+25}_{-40}K, respectively; (3) the corresponding extremum number densities at 50 km are $3.4^{+4.0}_{-0.1} \times 10^{13}$ cm^{-3} and $2.8^{+1.2}_{-0.8} \times 10^{13}$ cm^{-3}, respectively; (4) the corresponding extremum temperature gradients are 0.65 K km^{-1} and 0.55 K km^{-1} (±10%), respectively. It is clear that such a density profile cannot produce the knife edge *A*.

Since the stellar occultation experiment was performed for essentially the same latitude (and about the same time—within four months) of the Voyager 1 solar occultation experiment, it is possible to correlate the results from the two sets of data. The solar occultation data indicated that a column density of 3×10^{16} cm^{-2} was reached in a region where the scale height was essentially constant (the H_2 molecules have an absorption cross section of about 10^{-17} cm^2 in the 665–692 Å wavelength interval for which a 26% absorption of the solar signal was observed [*Atreya et al.*, 1979]).

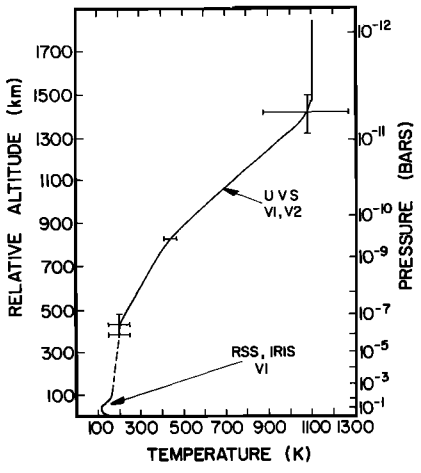

Fig. 7. Temperature as a function of altitude above the ammonia cloud tops (left ordinate) and pressure (right ordinate) as deduced from the various Voyager experiments. The broken line is the extrapolation of the UVS α Leo data to the IRIS and RSS data.

Our study of the 50–500 km region provides temperature gradients which are valid in the first few hundred kilometers above the 500 km level since it is this part of the atmosphere which determines the absorption at the 500 km level. A minimum gradient of 0.5 K km^{-1} has been found when the altitude of the turnaround point is 50 km. This minimum acceptable value increases when the altitude of the turnaround point increases. No reliable upper limit of the gradient can be found using these data, since the values which are found increase continuously with the altitude of the turnaround point. The reason is that the shorter the portion of the light curve which is used for the slope determination, the worse is the accuracy of the value determined. Therefore, we use the following technique for determining the upper limit of the temperature gradient above 500 km. We have tested various linearly increasing temperature profiles in the region above 500 km using the following boundary conditions:

1. The temperature at 500 km is 425 ± 25 K, and the density at this level is $5^{+6}_{-2} \times 10^9$ cm^{-3}.
2. No significant absorption is detected at the 1000 km level; i.e., absorption is less than 5%.
3. The temperature is 1100 ± 200 K where the line of sight column density is 3×10^{16} cm^{-2}, based on the Voyager 1 solar occultation data. It should be noted that further analysis of the Voyager 1 solar occultation data including the effects of short wavelength internal scattering have lowered the temperatures reported in *Atreya et al.* [1979]. The new value, 1100 ± 200 K, is, however, within the range of statistical uncertainties of the previous values and the equatorial RSS data.

The combination of constraints 2 and 3 results in a maximum temperature gradient of 1.6 K km^{-1}.

Figure 7 shows the complete temperature profile together with measurements obtained by the Voyager 1 solar occultation experiment, and IRIS experiments [*Eshleman et al.*, 1979; *Lindal et al.*, 1981; *Hanel et al.*, 1979]. The heights are measured from the ammonia cloud tops located at $p \approx 600$ mbar, $T = 150$ K; the corresponding pressures are shown on the right ordinate. The altitude reference Z_{t_0} used in the discussion of the data of Figures 1–5 earlier is found to be approximately 330 km above the ammonia cloud top altitude reference. The broken line represents extrapolation of the α Leo UVS data to the IRIS and RSS data. Since no definite information on the temperature structure in the 10 μbar to 1 mbar region is available, a linear temperature gradient is just as good an assumption as any. Our conclusions about the hydrocarbon mixing ratios and the eddy diffusion coefficient are little affected provided the average temperature in this region lies in the 150–200 K range.

2. *Hydrocarbons*

A close examination of Figure 6 shows that the absorption by H_2 above 1200 Å is completely negligible unless the temperature is at least 500 K and the line of sight column density as high as 10^{20} cm^{-2}. When the line of sight crosses the 330 km level, the column density (computed with the parameters determined above (section D1)) is about 7×10^{22} cm^{-2} but the number of molecules having a temperature of 500 K or higher is around 4×10^{18} cm^{-2} precluding significant H_2 absorptions at $\lambda > 1200$ Å. Hydrocarbons are the most likely absorbers in the Jovian atmosphere above 1200 Å. We shall examine by using Figure 5 the role of the potential absorbers, CH_4, C_2H_6, C_2H_2, and C_2H_4 in producing the observed absorption. The following information contained in Figure 5 will be useful: (1) three knife edge effects occur in the 1100–1190 Å (*A*), 1265–1320 Å (*B*), and 1365–1410 Å (*C*) wavelength intervals, (2) two plateaus are well defined in the 1310–1360 Å and in the 1430–1480 Å wavelength intervals, and (3) the general trend indicated by the broken line is that a deeper absorption level is reached with increasing wavelength.

In order to interpret these characteristics, we first consider three possible absorbers, namely, methane (CH_4), ethane (C_2H_6), and acetylene (C_2H_2). The case of ethylene (C_2H_4) will be examined later in this section. Their absorption cross sections taken from *Okabe and Becker* [1963], *Mount et al.* [1977], and *Nakayama and Watanabe* [1964] are shown in Figure 5. Figure 8 shows the maximum column densities (taking into account the altitude uncertainty) of these absorbers which are required to explain the features of Figure 5 if a given species were the only absorber. Whatever the number of species absorbing at a given wavelength, a knife edge effect is produced when a strong variation of the column density occurs. The *A* and *B* knife edges occur at an altitude (within the altitude uncertainty) which does not depend on the absorbing wavelength: this indicates a relatively constant cross section for the absorber over the wavelength intervals of occurrence of these knife edges. C_2H_2 can, therefore, be excluded, while, C_2H_6 is still a possible candidate if the scale height is of the order of 5 km or less. The knife edge *C* occurs over a 15 km altitude range and the absorption wavelength varies over 40 Å. In order to maintain the existence of the knife edge, the variation of the cross section of the absorber over these 15 km should be compensated by a corresponding variation of the column density. Since the column density decreases with decreasing wavelength (or increasing altitude), the cross section of the absorber should vary in the opposite direction. These variations are 7 and 1.6 for CH_4 and C_2H_6, respectively. In other words, the scale heights should be at most 5 and 21 km in order to produce the required compensations. But it should be noted that to produce a knife edge at a given wavelength, the absorption should increase from approximately 20% to 80% within a 10 km altitude range, this corresponds to an increase of the column density by a factor of 7. Consequently, C_2H_6 cannot produce the knife edge *C*.

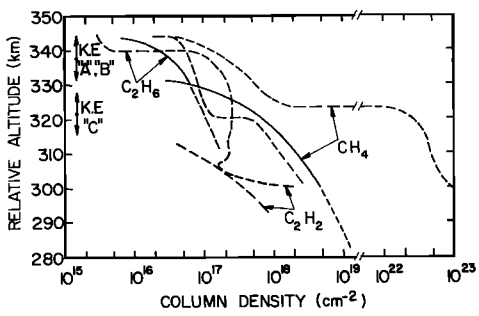

Fig. 8. Maximum column densities (dashed lines) required to produce the observed absorption assuming a single absorber. The full lines represent the actual column density profiles determined as explained in the text. The altitude ranges of the three knife edges *A*, *B*, and *C* are shown by the vertical arrows.

Finally, in order to calculate the various line of sight column density profiles which are shown in Figure 8 we have added the following constraints on the possible profiles:

1. In order to produce 50% absorption by a single absorber, we find that the C_2H_6 line of sight column density at 208 km must be $3^{+2}_{-2} \times 10^{16}$ cm^{-2}, and that the CH_4 line of sight column density at 192 km must be $5^{+6}_{-3} \times 10^{17}$ cm^{-2}. The error bars reflect the altitude uncertainties.

2. The scale height has been assumed to increase linearly with decreasing altitude. By varying the rate of increase, various column density profiles are obtained and compared to the data.

The fitting procedure consists of comparing the computed line of sight density profiles with the data, i.e., the C_2H_6 knife edges, *A* and *B*, should occur over a few kilometers altitude interval at most and the C_2H_6 absorption should not be significant 16 km below, while the CH_4 knife edge, *C*, should occur over a ~15 km altitude interval and the CH_4 absorption at 208 km should be neglible. The results are displayed in Figure 8 (column density profiles) and Figure 9 (number density profiles). One notes in Figure 8 that at the altitude of the knife edges the scale height is approximately 6 km; the main difference between the C_2H_6 and CH_4 profiles lies in the rate of increase of the scale height while the altitude decreases. As an example, scale heights of 20 km are reached respectively 5 and 25 km below the knife edge levels in the C_2H_6 and CH_4 cases. These two profiles cannot be extrapolated below these levels since the (unknown) rate of increase of the scale height becomes very small when the optical depth increases.

The CH_4 and C_2H_6 distributions determined above cannot produce a sufficient absorption in the 290–310 km altitude range. We attribute this deficiency to the lack of C_2H_2 in the model. Since, in the data, there is an indication that a knife edge exists around 1520 Å (and in the 300–310 km altitude range), we have evaluated the C_2H_2 column density assuming that the scale height was 6 km at 305 km and had the same variation with altitude as the CH_4 column density. The column densities were scaled in order to produce a total absorption of 50% at the 305 km level. The value given for C_2H_2 represents only an upper limit. It is fair to say that the C_2H_2 upper limit determined here is at best a rough value.

Among the stable hydrocarbons likely to be present in the Jovian upper atmosphere and not considered in the above analysis, only ethylene (C_2H_4) has a significant absorption cross section in the 1200–1600 Å interval. We have ruled out C_2H_4 as an absorber in the 310–350 km region for the same reason we have rejected C_2H_2, i.e., the absorption cross section is such that a knife edge would be observed at the same altitude throughout the 1100–1600 Å region. On the other hand, C_2H_4 cannot be the absorber we require above 1500 Å either

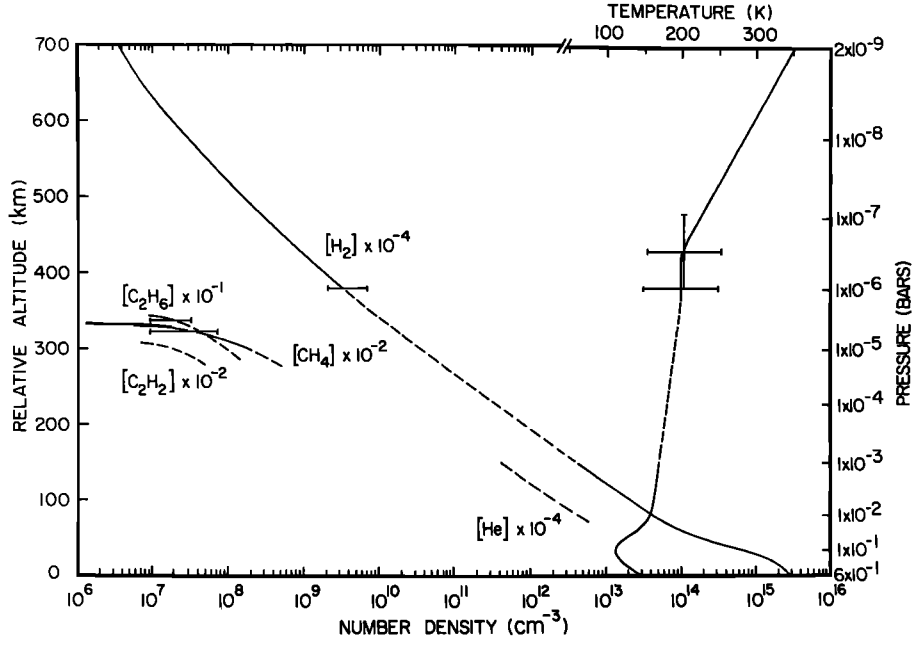

Fig. 9. H_2, CH_4, C_2H_6, and C_2H_2 density profiles, as well as the neutral temperature structure derived from the analysis of the α Leo occultation experiment. C_2H_2 density is an upper limit. The temperature gradient is ~1 K km^{-1} above 800 km. All altitudes are relative to the ammonia cloud tops located at $P = 600$ mbar, $T = 150$ K. Pressures on the right ordinate correspond to the altitudes on the left ordinate. The broken line in the temperature profiles shows extrpolations to the IRIS and RSS measurements. Helium density is simply a representation of the IRIS measurement of the homospheric mixing ratio for He [*Atreya et al.*, 1981].

since the absorption cross section increases with increasing wavelength and consequently the absorption at the higher altitudes should take place in the longer wavelengths. In other words, assuming that C_2H_4 would produce the required absorption around 1550–1600 Å, there would be no way to produce any significant absorption around 1500 Å at the same altitude, and evidently no knife edge would be produced.

The various uncertainties in our calculations translate into an uncertainty of about a factor of 2 in the number densities (and into the uncertainties already mentioned in the column densities), while the C_2H_2 density is an upper limit. The α Leo data yield mixing ratios at 325 km (~5 μbar) of $2.5^{+3}_{-2} \times 10^{-5}$ and $2.5^{+2.0}_{-1.5} \times 10^{-6}$ for CH_4 and C_2H_6, respectively. The upper limit for the mixing ratio of C_2H_2 is 5×10^{-6} at 300 km (~10 μbar).

E. DISCUSSION

For a detailed discussion of the theoretical implications of the results obtained in this paper, the reader is referred to a paper by *Atreya et al.* [1981].

In Figure 7 the thermal structure from the ammonia cloud tops to 1 mbar level ($z \approx 150$ km) is from the Voyager RSS and IRIS measurements [*Eshleman et al.*, 1979; *Lindal et al.*, 1981; *Hanel et al.*, 1979, 1980]. The general structure of this region was also known from the ground based measurements. Within the range of statistical uncertainties, most of the ground based visible stellar occultation data agreed on a temperature of 170 ± 30 K at 10 μbar level (see review by *Hunten and Veverka* [1976] and *Hunten* [1976]). The neutral temperature in the 1500 km height range has been determined by the Voyager 1 solar occultation experiment [*Atreya et al.*, 1979]. As noted earlier, further analysis of the solar occultation data including the scattering corrections lower the Atreya et al. exospheric temperature value somewhat so that the exospheric neutral temperature is found to be in general agreement with the equatorial plasma temperature (1200–1300 K) deduced from the electron density profiles [*Eshleman et al.*, 1979]—implying equilibrium between the neutral gas and plasma at these heights.

Before the Voyager α Leo data, no information on the temperature gradient in the pressure region below 10 μbar was available, and it was not obvious how far below the 10 μbar level the ground based visible stellar occultation data were valid. The new data discussed in this paper have provided a temperature profile in $P \lesssim 1$ μbar region. The average lapse rate above 400 km ($P \gtrsim 1$ μbar) is found to be about -1 K km^{-1} in the present paper. In order to reconcile the upper atmospheric hydrocarbon densities determined in this paper with their stratospheric values, the temperature in the 1 μbar to 1 mbar range must be confined to 170 K to 200 K. Indeed, the visible stellar occultation data [see *Hunten*, 1976] can, with some caution, be extended from 10 μbar to 1 mbar level to give a nearly isothermal mesosphere.

Prior to the determination of the thermospheric temperature gradient, it was thought that the inertia gravity waves could supply the needed energy to heat the upper atmosphere. Indeed, the solution of the appropriate heat conduction equation by *Atreya et al.* [1979] and *Atreya and Donahue* [1976] indicated that these waves could easily raise the temperature above the homopause to 1000–1500 K. However, the thermospheric temperature gradient found in this paper cannot be reconciled with a much faster temperature rise above the homopause expected from the dissipation of such waves. Moreover, it is not apparent where the waves would break up, and whether they would subsequently dissipate their energy as heat or be simply reflected.

Joule heating, precipitation of magentospheric electrons (soft and hard), as well as solar EUV remain as potential candidates—although any particular source is difficult to reconcile with many observed atmospheric phenomena on Jupiter. We conclude that upper atmospheric heating and its temporal variation is caused by a mechanism which tends to deposit heat quite high in the atmosphere and appears to be related to the solar activity.

The other important aeronomic parameter on which the stellar occultation data have shed light is the value of the mixing parameter—eddy diffusion coefficient, K_h, at the homopause. It has been generally assumed that if one is able to determine the density distribution of the heavier gases in an atmosphere, one can in effect ascertain the homopause level, since the heavier gases will drop in density above this level. Once this level is known, determination of the eddy diffusion coefficient, K_h, is a simple exercise. At the homopause, the molecular diffusion coefficient D is equal to the eddy diffusion coefficient K. This situation may be complicated due to the photolysis and possible charged particle destruction of the hydrocarbons which may tend to reduce their densities much below the mathematically defined level of the homopause. However, in the equatorial region for which these data are presented, it is quite unlikely that charged particle precipitation and subsequent destruction of methane would be important. An analysis involving photochemistry of methane has been carried out by *Atreya et al.* [1981], to discern the value of K_h, and it is found to be $1.4^{+0.8}_{-0.7} \times 10^6$ cm^2 s^{-1} which is consistent with the value of $\sim 10^6$ cm^2 s^{-1} deduced from the Voyager Lyman α and He 584 Å airglow emissions measured at the same time [*Broadfoot et al.*, 1981; *McConnell et al.*, 1981].

The volume mixing ratios of CH_4 and C_2H_6 at 325 km (5 μbar) are found to be 2.5×10^{-5} and 2.5×10^{-6}, while the upper limit for the C_2H_2 mixing ratio at 300 km (~10 μbar) is 5×10^{-6}. The IRIS data [*Hanel et al.*, 1979; *Gautier et al.*, 1980] indicate the mixing ratios to be $(1.4 \pm 0.45) \times 10^{-3}$, 5×10^{-6}, and 3×10^{-8} to 10^{-7} for CH_4, C_2H_6, and C_2H_2, respectively, at much deeper levels in the Jovian stratosphere. The IRIS data are being further analyzed (D. Gautier, personal communication, 1980), to determine the volume mixing ratios of the hydrocarbons at the heights which overlap with the UVS data. The upper atmospheric mixing ratios are expected to be different from the stratospheric values because of photolysis at the higher elevations.

We do not show a density profile for atomic hydrogen in Figure 9 since the Lyman alpha airglow data give only its total column abundance (1×10^{17} cm^{-2}) above the methane absorption layer [*McConnell et al.*, 1980]. This too is an approximate value since resonance scattering of the solar Lyman α photons was considered to be the sole source of the Jovian dayside Lyman α emission. The observed nightglow of Lyman α [*Broadfoot et al.*, 1981], hydrogen bulge [*Sandel et al.*, 1979; *Dessler et al.*, 1981], H_2 Lyman and Werner band emission characteristics [*Shemansky et al.*, 1981] challenge this assumption.

Acknowledgments. This work was supported by a grant from the Planetary Atmospheres Program of the NASA Solar System Exploration Division, and by NASA Voyager contract NAS 7-100, through the Jet Propulsion Laboratory. We acknowledge the National Center

for Atmospheric Research for computer time for some of the calculations reported in this paper.

REFERENCES

Allison, A. C., and A. Dalgarno, Band oscillator strengths and transition probabilities for the Lyman and Werner systems of H_2, HD and D_2, *At. Data, 1,* 289, 1970.

Atreya, S. K., and T. M. Donahue, Model ionospheres of Jupiter, in *Jupiter*, edited by T. Gehrels, pp. 304–318, University of Arizona Press, Tucson, Ariz., 1976.

Atreya, S. K., T. M. Donahue, B. R. Sandel, A. L. Broadfoot, and G. R. Smith, Jovian upper atmospheric temperature measurement by the Voyager 1 UV spectrometer, *Geophys. Res. Lett., 6,* 795–798, 1979.

Atreya, S. K., T. M. Donahue, and M. C. Festou, Jupiter: Structure and composition of the upper atmosphere, *Astrophys. J. Lett., 247,* in press, 1981.

Broadfoot, A. L., and B. R. Sandel, Self-scanned anode array with a microchannel plate electron multiplier, *Appl. Opt., 16,* 1533, 1977.

Broadfoot, A. L., B. R. Sandel, D. E. Shemansky, S. K. Atreya, T. M. Donahue, J. L. Bertaux, J. E. Blamont, D. F. Strobel, J. C. McConnell, H. W. Moos, R. Goody, A. Dalgarno, M. B. McElroy, and Y. L. Yung, Ultraviolet spectrometer experiment from the Voyager mission, *Space Sci. Rev., 21,* 183–205, 1977.

Broadfoot, A. L., M. J. S. Belton, P. Z. Takacs, B. R. Sandel, D. E. Shemansky, J. B. Holberg, J. M. Ajello, S. K. Atreya, T. M. Donahue, H. W. Moos, J. L. Bertaux, J. E. Blamont, D. F. Strobel, J. C. McConnell, A. Dalgarno, R. Goody, and M. B. McElroy, Extreme ultraviolet observations from Voyager 1 encounter with Jupiter, *Science, 204,* 979–982, 1979.

Broadfoot, A. L., B. R. Sandel, D. E. Shemansky, J. C. McConnell, G. R. Smith, J. B. Holberg, S. K. Atreya, T. M. Donahue, D. F. Strobel, and J. L. Bertaux, Overview of the Voyager ultraviolet spectrometry results through Jupiter encounter, *J. Geophys. Res.*, in press, 1981.

Cook, A. F., T. C. Duxbury, and G. E. Hunt, A lower limit on the top of Jupiter's haze layer, *Nature, 280,* 781, 1979.

Dabrowski, I., and G. Herzberg, The absorption spectrum of D_2 from 1100 to 840 Å, *Can. J. Phys., 52,* 1110, 1974.

Dalgarno, A., and T. L. Stephens, Discrete absorption of molecular hydrogen, *Astrophys. J., 160,* L107, 1970.

Dessler, A. J., B. R. Sandel, and S. K. Atreya, The Jovian hydrogen bulge: Evidence for a co-rotating magnetospheric convection, *Planet. Space Sci., 29,* 215, 1981.

Eshleman, V. R., G. L. Tyler, G. E. Wood, G. F. Lindal, J. D. Anderson, G. S. Levy, and T. A. Croft, Radio science with Voyager 1 at Jupiter: Preliminary profiles on the atmosphere and ionosphere, *Science, 204,* 976, 1979.

Gautier, D., R. Hanel, B. Conrath, V. Kunde, W. Maguire, A. Chen, N. Husson, N. Scott, J. P. Baluteau, A. Marten, and D. Rouan, Mixing ratios of the main atmospheric components of Jupiter from Voyager infrared measurements, paper presented at the XXIII COSPAR Meeting, Budapest, Hungary, June 1980.

Hanel, R. A., B. Conrath, M. Flaser, V. Kunde, P. Lowman, W. Maguire, J. Pearl, J. Pirraglia, R. Samuelson, D. Gautier, P. Gierasch, S. Kumar, and C. Ponnamperuma, Infrared observations of the Jovian system from Voyager 1, *Science, 204,* 972–976, 1979.

Hanel, R., B. Conrath, M. Flaser, V. Kunde, W. Maguire, J. Pirraglia, R. Samuelson, D. Gautier, and P. Gierasch, Energy balance, composition, thermal structure and dynamics of the Jovian atmosphere derived from the Voyager infrared investigation, paper presented at the XXIII COSPAR Meeting, Budapest, Hungary, June 1980.

Herzberg, G., Molecular spectra and molecular structure, in *Spectra of Diatomic Molecules*, Van Nostrand, New York, 1959.

Herzberg, G., and L. L. Howe, The Lyman bands of molecular hydrogen, *Can. J. Phys., 37,* 636, 1959.

Hunten, D. M., Atmospheres and ionospheres, in *Jupiter*, edited by T. Gehrels, pp. 22–31, University of Arizona Press, Tucson, Ariz., 1976.

Hunten, D. M., and J. Veverka, Stellar and spacecraft occultations by Jupiter: A critical review of derived temperature profiles, in *Jupiter*, edited by T. Gehrels, p. 247, University of Arizona Press, Tucson, Ariz., 1976.

Lindal, G. F., G. E. Wood, G. S. Levy, J. D. Anderson, D. N. Sweetnam, H. B. Hotz, B. J. Buckles, D. F. Holmes, P. E. Doms, V. R. Eshleman, G. L. Tyler, and T. A. Croft, The atmosphere of Jupiter: An analysis of the Voyager radio occultation measurements, *J. Geophys. Res.*, in press, 1981.

McConnell, J. C., B. R. Sandel, and A. L. Broadfoot, Airglow from Jupiter's night side and crescent: Ultraviolet spectrometer observations from Voyager 2, *Icarus, 43,* 123, 1980.

McConnell, J. C., B. R. Sandel, and A. L. Broadfoot, Voyager UV spectrometer observations of He 584 Å airglow at Jupiter, *Planet. Space Sci.*, in press, 1981.

Mount, G. H., E. S. Warden, and H. W. Moos, Photoabsorption cross sections of methane from 1400–1850 Å, *Astrophys. J., 214,* L47–L49, 1977.

Nakayama, T., and K. Watanabe, Absorption and photoionization coefficients of acetylene, propyne and 1-Butyne, *J. Chem. Phys., 40,* 558–561, 1964.

Namioka, T., Absorption spectra of H_2 in the vacuum ultraviolet region, I, The Lyman and Werner bands, *J. Chem. Phys., 40,* 3154, 1964.

Okabe, H., and D. A. Becker, Vacuum-ultraviolet photochemistry, VII, Photolysis of *m*-butane, *J. Chem. Phys., 39,* 2549–2555, 1963.

Sandel, B. R., D. E. Shemansky, and A. L. Broadfoot, Observations of the diffuse interstellar EUV radiation field, *Astrophys. J., 227,* 808–815, 1979.

Sandel, B. R., A. L. Broadfoot, and D. F. Strobel, Discovery of a longitudinal asymmetry in the Lyman alpha brightness of Jupiter, *Geophys. Res. Lett., 7,* 5–8, 1980.

Shemansky, D. E., Transition probabilities and collision broadening cross-section of the N_2 Lyman-Birge-Hopfield systems, *J. Chem. Phys., 51,* 5487, 1969.

Shemansky, D. E., B. R. Sandel, and A. L. Broadfoot, Voyager observations of the interstellar medium in the 500 to 1700 Å spectral region, *J. Geophys. Res., 84,* 139–142, 1979.

Shemansky, D. E., J. C. McConnell, B. R. Sandel, and A. L. Broadfoot, Excitation of H_2 Lyman and Werner bands on Jupiter, Space Sci. Inst., Univ. of S. Calif., Tucson, Ariz., 1981.

Smith, D. W., T. F. Greene, and R. W. Shorthill, The upper Jovian atmosphere aerosol content determined from a satellite eclipse observation, *Icarus, 30,* 697–729, 1977.

Wilkinson, P. G., The electronic isotope shift in the Lyman bands of H_2, HD and D_2, *Can. J. Phys., 46,* 1225, 1968.

(Received November 3, 1980;
revised January 30, 1981;
accepted February 24, 1981.)